Received: 7 May 2022 | Revised: 30 June 2022 | Accepted: 6 August 2022

DOI: 10.1002/nano.202200092

RESEARCH ARTICLE

Nano Select Open Access WILEY

Designed assembly and disassembly of DNA in supramolecular structure: From ion regulated nuclear formation and machine learning recognition to running DNA cascade

Timur A. Aliev[1] | **Alexandra A. Timralieva**[1] | **Tatiana A. Kurakina**[1] | **Konstantin E. Katsuba**[1] | **Yulia A. Egorycheva**[1] | **Mikhail V. Dubovichenko**[1] | **Maxim A. Kutyrev**[1] | **Vladimir V. Shilovskikh**[1] | **Nikita Orekhov**[2,3,4] | **Nikolay Kondratyuk**[2,3,5] | **Sergey N. Semenov**[6] | **Dmitry M. Kolpashchikov**[1,7,8] | **Ekaterina V. Skorb**[1]

[1]ITMO University, Saint Petersburg, Russia

[2]Moscow Institute of Physics and Technology, Moscow, Russia

[3]Joint Institute for High Temperatures of the Russian Academy of Sciences, Moscow, Russia

[4]Bauman Moscow State Technical University, Moscow, Russia

[5]National Research University Higher School of Economics, Moscow, Russia

[6]Department of Molecular Chemistry and Materials Science, Weizmann Institute of Science, Rehovot, Israel

[7]University of Central Florida, Chemistry Department, Orlando, Florida, USA

[8]Burnett School of Biomedical Sciences, University of Central Florida, Orlando, Florida, USA

Correspondence
Ekaterina V. Skorb, ITMO University, Lomonosova str. 9, 191002 Saint Petersburg, Russia.
Email: skorb@itmo.ru

Funding information
Ministry of Science and Higher Education of the Russian Federation, Grant/Award Number: 075-15-2021-1349

Abstract

In this paper, we introduce a novel encapsulation system for DNA oligonucleotides. Supramolecular assembly of melamine cyanurate encapsulates DNA at pH 7 and start to release it at pH less than 6.5. We study the assembly and disassembly in time in specially designed reaction-diffusion system. Magnesium ions allow spatial separation of DNA with the highest DNA concentration in the core of melamine cyanurate capsule. Molecular dynamics (MD) simulation shows that DNA acts as a nucleation centre for melamine cyanurate. Dataset of fluorescent images analysed by machine learning algorithms indicates correlation between structure of melamine cyanurate capsules for DNA trapping and concentration of magnesium ions. The concentration of magnesium ions can be recognized with 96% accuracy proving that all environmental conditions are extremely important during the self-assembly and should be considered for laboratory and industrial applications of the suggested approach. Moreover, the

encapsulated DNA can undergo a cascade reaction consisting of hybridization with complementary strand and its cleavage at a designated site. This reactivity opens a fresh avenue for various applications in biosensing, diagnostics, DNA compartmentalization, and even gives new hints for the origin-of-life questions.

KEYWORDS

DNA cascade, encapsulation, machine learning, nucleation, self-assembly, supramolecular structure

1 | INTRODUCTION

DNA oligonucleotides (ssDNA) are used as primers and probes in diagnostics,[1] biosensing,[2] and bioanalysis.[3] ssDNA is a material used by DNA nanotechnology for building nanostructures with shapes tailored to specific applications. These shapes are programmed using rules of complementary base paring.[4,5] Furthermore, DNA is used to create signaling and information processing circuits that regulate communication between protocells[6] and artificial cells[7] and enable DNA-based data storage.[8]

The strict requirements for ssDNA storage conditions limit its applicability in many studies.[9] Generally, ssDNA storage goes through a few preliminary costly procedures such as freeze-drying.[10] In case of a long-term storage, the most important requirement is constant low temperature.[11] The buffer solution, essential for most implementations, also effects ssDNA if it is undried.[12] Therefore, the question is how to simplify procedure for ssDNA storage remains open.

Currently, promising approaches to ssDNA storage are to incorporate ssDNA into protecting shells such as lipid[13] or hybrid capsules.[14] One of the most effective techniques is a layer-by-layer ssDNA loading.[15–20] It provides the DNA loading through cyclic bilayer formation and, finally, protection shell formation. Despite the high percent of ssDNA loaded, the procedure is time consuming. Besides, several difficult procedures such as moderate heat-treating combined with high humidity can trigger the shell destruction and DNA release. Several solid host can load DNA without bicyclic layer formation, such as cationic nanoparticles.[21] These solid host provide protection without any extra protective outer layer. Thus, these solid hosts are chosen specifically to an encapsulated substance and hardly applicable for a wide range of reagents.[22]

Another approach is post-formation ssDNA-loading, typically performed by metal-organic frameworks.[23] The main requirement is a positive charge of the metal-organic framework to provide DNA-loading. These frameworks effectively capture ssDNA from solutions and store it in pores,[24] but the DNA release requires immersing the material in the solution of complementary DNA strands. Another release triggers such as heat and pH change are not applied yet.

Stimuli-responsive release of an encapsulated compound is one of the most important requirements to the capsules with the reversible chemical bonding such as hydrogen bonding.[25] Melamine (M) cyanurate (CA) supramolecular assemblies (M-CA) are pH-sensitive,[26] which is a significant advantage for release. Modified M and CA are considered as prebiotic nucleotides.[27] The unique structure and properties of these molecules allow them to bind assemblies with DNA. For example, Li et al. has created a poly(thymine) – M duplex.[28] Another study by Avakyan et al. has programmed poly(adenine)-CA fibers.[29] No one has tried to create an assembly from M, ssDNA, and CA so far.

Moreover, these supramolecular assemblies can encapsulate organic molecules[30] opening further avenue for co-loading the structure. Importantly, the loaded substances engage in the nucleation process and affect the further supramolecular crystal growth.[31] A model reaction-diffusion system in gel is used for in time controlling the process of assembly.[32] It opens the way to indicate the effect of environmental conditions on the self-assembly.

In this paper, we perform melamine cyanurate supramolecular capsules that self-assemble with ssDNA. Ion regulation of capsules' formation is performed, and artificial intelligence methods are applied to identify the effect of environment conditions. We demonstrate that these capsules can transform under pH change and enable running of DNA cascade in gels.

2 | RESULTS AND DISCUSSION

We used the reaction-diffusion process for capsules formation. The schematic experiment is shown in Figure 1A, and gel preparation is shown in Figure S1. We fabricated agar gels of three initial reactants in special reservoirs and cut

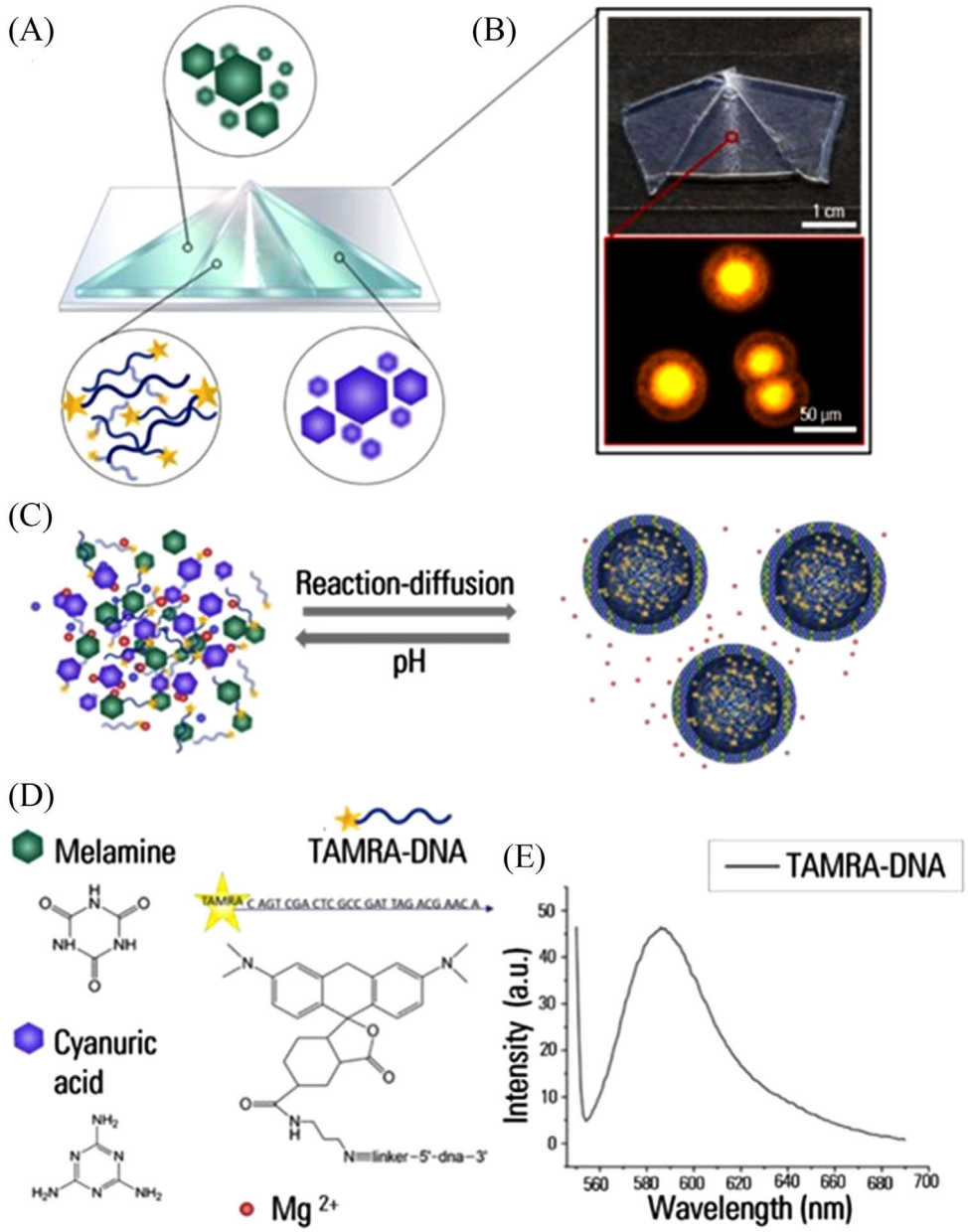

FIGURE 1 Reaction-diffusion system for ssDNA encapsulation. A, 1 wt % agar gels containing 13 mM melamine (M), 100 nM ssDNA, and 13 mM cyanuric acid (CA) present in the system (from the left to the right). B, The upper image shows melamine cyanurate (M-CA) capsules formed within the ssDNA containing gel during the reaction-diffusion process at specially design system. The bottom image shows M-CA capsule with incorporated ssDNA in RHOD channel. C, M-CA capsules' assembly in the presence of 50 mM Mg^{2+} during reaction-diffusion process and its disassembly after pH change. D, Molecular structures of the components. E, Fluorescence spectrum of the TAMRA fluorophore.

them as triangles. The reaction-diffusion system consists of three connected segments where the encapsulated reactant is in the middle. M and CA diffusing fronts cross at different times in top and the bottom of ssDNA gel triangle, as the space between M and CA is different. The capsules form strictly in between, and with the increase of interspace the capsules form slower. Thus, it is easy to observe capsules formation from the beginning to the end due to the triangular cut of agar gels. We observe local formation of white capsules at the crossing of diffusing reactants fronts and see surprisingly bright luminescence of the capsules (Figure 1B). Reaction-diffusion system is reversible and with pH change the capsules disassemble with release of all constituents, as shown in Figure 1C. We investigate the system consisting of M, CA, modified ssDNA and Mg^{2+} (Figure 1D). ssDNA is modified with TAMRA fluorophore to monitor how the encapsulation goes (Figure 1E, Figure S2). M-CA particles did not show significant luminescence

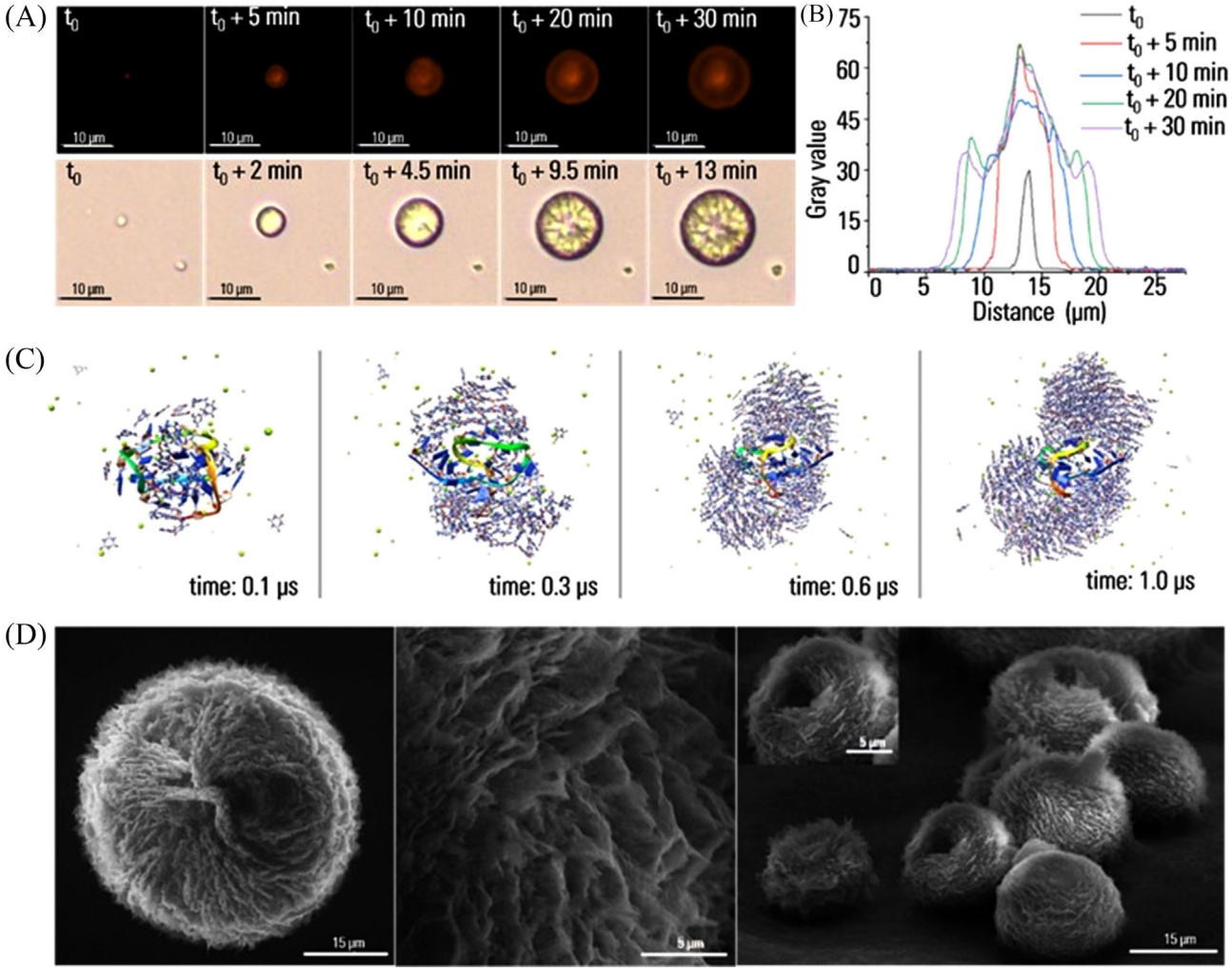

FIGURE 2 Capsule formation during nucleation and post-nucleation. A, Images of the M-CA capsules' assembly in RHOD channel at different reaction times. B, Fluorescence intensity profile during formation of the M-CA capsule, the profile is built through the center of the capsule. C, Time-dependent fluorescence microscopy images of the capsule in bright field (BF). D, Snapshots of molecular dynamics (MD) computational cell for Mg^{2+}-containing system along the process of ssDNA-M-CA cluster formation (green spheres represent Mg^{2+} ions, water molecules are not shown). E, Scanning electron microscopy images of the capsules.

in red fluorescence channel (excitation 546 nm, emission 585 nm, RHOD) (Figure S3) without ssDNA.

To investigate the details of the assembly dynamics, we performed a serious of time-dependent experiments (Figure 2A, see also Supplementary Videos 1, 2) with sequential imaging of an assembled particle in bright field (BF) (over the first 13-minute period of formation Video 1) and fluorescent modes (over the first 30 minutes Video 2). Profiles of fluorescence are presented in Figure 2B. The center of the formation capsule is a bright one. This fluorescence distribution is constant for the same experimental conditions, for example 50 mM Mg^{2+} ion concentration.

Within the classical molecular dynamics (MD) approach, we analyzed the process of M-CA assembly in an aqueous solution (Figure 2C) in the presence of Mg^{2+} ions (details on the MD simulations and methods of analysis are presented in the Supporting Information). The corresponding movie of MD simulations is also available in Supplementary Video 3.

The formed M-CA-ssDNA capsules have a repeated donut-like shape, average size is 35–50 μm (Figure 3D). The capsules consist of platy flakes with estimated thickness about 100 nm. The capsules have pronounced growth center and several growth planes in contrast to pure melamine cyanurate crystals with needle-like shape,[25] that suggests impact of the ssDNA on the nucleation process.

2.1 | Ion regulated capsule formation

The luminescence intensity of encapsulated ssDNA and its distribution among M-CA depended on

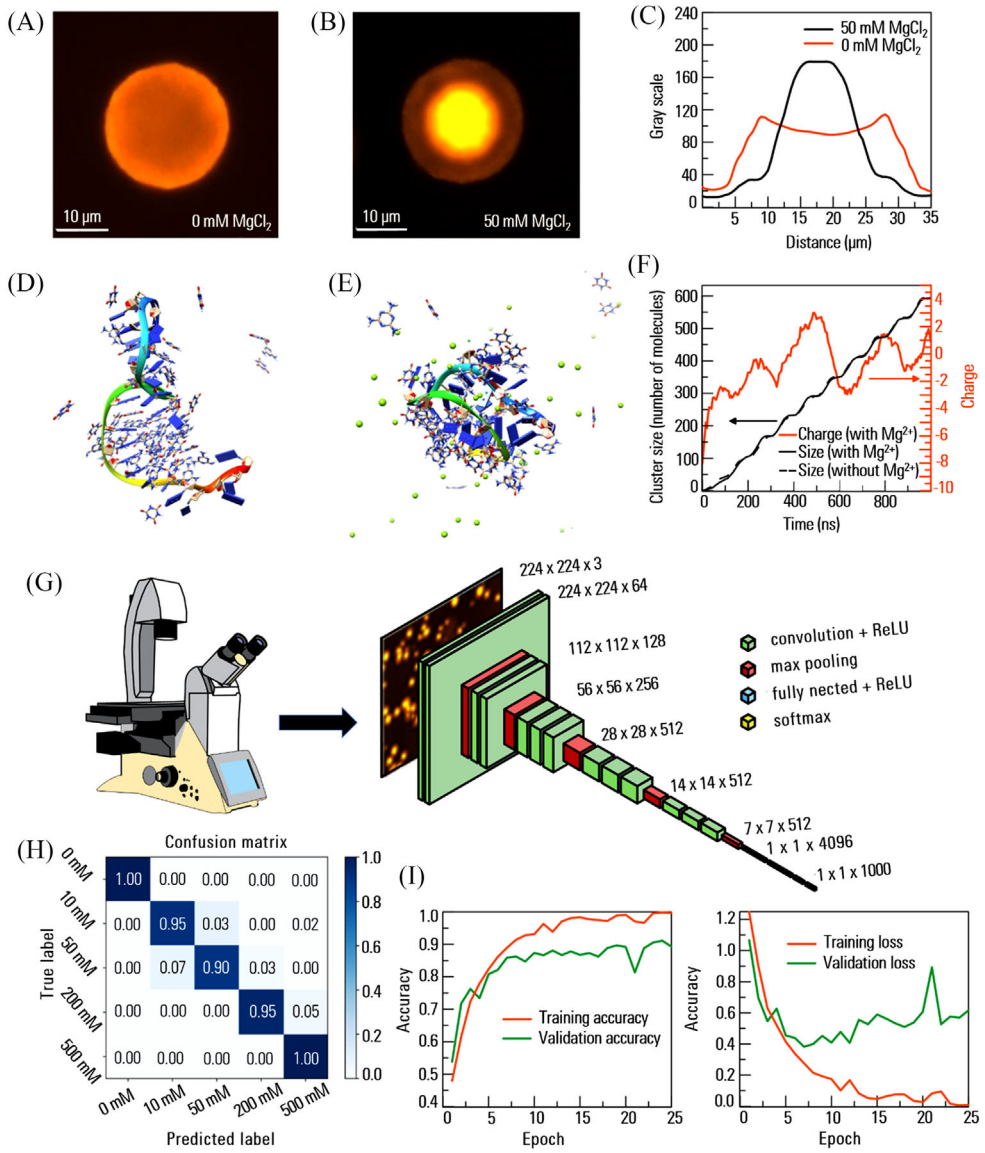

FIGURE 3 Environmental conditions effect recognition. A, Fluorescence of the capsule without Mg^{2+} in RHOD channel. B, Fluorescence of the capsule in presence of 50 Mm Mg^{2+} in RHOD channel. C, Averaged fluorescence intensity profiles of the capsules with and without magnesium in RHOD channel. D,E, Representative shortcuts from MD simulation of M, CA and DNA assembly in the absence (D), and in the presence of Mg^{2+} ions taken at $t = 0.1$ μs. F, Growth curves for molecular clusters formed in the presence (solid black) and in the absence (dashed black) of Mg^{2+}, the red curve shows a total charge of the cluster in Mg^{2+}-containing system. G, Fluorescent and optical microscopy data for VGG16 neural network. I, Confusion matrix for VGG16 neutral network. J, Plots of the ratio of training accuracy and validation accuracy (left), training loss and validation loss (right) for VGG16.

Mg^{2+}concentration. In biology, alkaline and alkaline earth metal ions, most importantly Mg^{2+} neutralize ssDNA's negative charge.[33]In the absence of Mg^{2+}, a fluorescence intensity of M-CA-ssDNA capsules is similar through the particle (Figure 3A). In contrast, in the presence of Mg^{2+}, capsules have pronounced bright center and pale edges in RHOD channel (Figure 3B).

The cross-sectional profile of fluorescence intensity along the particle diameter corresponds to the DNA distribution inside the melamine cyanurate capsules (Figure 3C). The presence of Mg^{2+} during assembly of M, CA with ssDNA leads to ssDNA localization in the capsule core. However, the outer layers of the capsules also show emission in RHOD channel but less intensive than capsules formed without Mg^{2+}.

Interestingly, the concentration of Mg^{2+} greatly affected the number of forming particles. The number of capsules decreased with the increase in Mg^{2+} concentration (Figure S5A). We vary Mg^{2+} concentration to show the ion regulation of capsule formation. In presence of 500 mM Mg^{2+} there are no particles in the bottom section of the reaction-diffusion system after 3 hours of formation in contrast

to the system with 50 mM Mg^{2+} (Figure S4). Moreover, Mg^{2+} affects the average size distribution of the particles (Figure S5B). Capsules formed in the absence of Mg^{2+} or in the presence of 50 mM Mg^{2+} have size of 20–30 μm. In contrast, the average size of the capsules formed in the presence of 500 mM of $Mg^{2+}$was equal or less than 10 μm.

To verify Mg^{2+} incorporation in the structure of M-CA together with DNA, the local elemental analysis was used. Energy dispersive X-ray (EDX) analysis was performed for both initial capsule, and one after its cutting in half ssDNA-loaded melamine cyanurate capsules as Mg^{2+} can incorporate in the center of the particle through the nucleation stage when it stabilized DNA. However, no traces of Mg^{2+}were observed inside the capsules (Figure S6). Figure S7 shows the presence of DNA in the capsules, and it increases with the increase in Mg^{2+} concentration.

Despite the similarities between the two systems mentioned above, high Mg^{2+} concentrations brought one significant difference to the process: they neutralized negative DNA charges during the early stages of molecular cluster formation. The total charge of the molecular cluster is close to zero in the Mg^{2+}-containing system: the initial negative charge of ssDNA is compensated by Mg^{2+} ions located near its surface.

To clarify the structure of the early M-CA/ssDNA aggregates on the molecular level and to investigate the role of Mg^{2+} in the nucleation process, we performed two microsecond-long MD simulations of M-CA-ssDNA assembly in aqueous solution: one in the presence of Mg^{2+} and one without the ions. In both scenarios DNA behaves as a center of nucleation for a molecular cluster (Figure 3D,E, Supplementary Videos 3, 4) and both growth curves are almost identical (Figure 3F). Small oscillations of the growth curves were the result of the periodic increase in M and CA concentrations in the simulation (see Methods). Analysis of the Hermans' orientation parameter (Figure S8) demonstrated that first layers of accommodated M-CA were disordered for both systems, but after the cluster reached the size of 300–400 molecules, they became more and more organized with a pattern similar to the rosette-like (typical for pure M-CA crystals[34]).

To prove that Mg^{2+} ions do not intercalate into the M-CA lattice and interact predominantly with ssDNA, we performed additional simulation of M-CA nanoparticle nucleation in the aqueous solution in the absence of ssDNA. The radial distribution function obtained between the center of mass of the formed M-CA nucleolus and Mg^{2+} ions (Figure S9) demonstrated that Mg^{2+} remained in the solution, that is M-CA nuclei were electrically neutral and did not incorporate any Mg^{2+} ions, which is in full agreement with the results of EDX analysis. For a better understanding of DNA-Mg^{2+} and M-CA-Mg^{2+} interactions in the solution, we calculate dimer existence autocorrelation function (DACF) for the three types of molecular complexes: M-Mg^{2+}, CA-Mg^{2+} and $ssDNA^{-}$-Mg^{2+} (the last is a negatively charged phosphate group of ssDNA). Mg^{2+} did not form any long-living complexes with individual M or CA molecules, while its interaction with ssDNA is much more stable (Figure S10).

Our MD simulations demonstrate that Mg^{2+} ions do not interfere with M-ssDNA or CA-ssDNA interactions. It could imply that they affect the nucleation and formation of the capsules enhancing only DNA-DNA interactions, which is consistent with the previous observations for self-assembled DNA-based systems.

2.2 | Prediction of Mg^{2+} concentration from fluorescent images by artificial intelligence

Our experimental system enables the monitoring of M-CA capsules formation, but the capsules differ in each gel section (Figure S11–S13). Systems containing Mg^{2+} ions and systems without it were visually different. However, the changes in Mg^{2+} concentration affected the reaction-diffusion system less pronouncedly. For quantitative recognition of Mg^{2+} effect we used convolutional neural networks (CNN) originally developed to work with pattern recognition.[35] To get high prediction accuracy we also use transfer learning method.[36]

For our dataset, we obtained 7000 fluorescent microscopy images (Figure S14) to confirm whether dependences between Mg^{2+} concentration and the structures of assembled capsules and their fluorescence intensities existed. We formed the reaction-diffusion systems containing 0 mM, 10 mM, 50 mM, 200 mM, or 500 mM Mg^{2+}. The concentration of Mg^{2+} affected the fluorescence distribution of the particle and particles' size and the number of particles in different sections of reaction-diffusion system. We used three pretrained CNNs within transfer learning method to study this effect as more effective versus traditional analytical methods.

Eighty percent of the dataset was used for training and the rest for validation. The graphic card GTX2060 Super was used to accelerate the training. Other hardware and software are listed in Supplementary information. Figure S15 shows the ratio of accuracy and loss in epochs for different pre-trained neural networks. We use VGG16, VGG19 and ResNet50. In this case, VGG16 performs the best results (Figure S16), so we decide to use it in the architecture of this network (Figure 3G). When testing predictive analytics, 60 images of each class are used. These images are not included in the training dataset and randomly selected. Table S1 and Figure S17 presents data on the accuracy of each of the pretrained neural

networks. The predictive analytics accuracy was 96% for VGG16(Figure 3H). Confusion matrix reflexes the relationship between true label and predictive label of each class. Thus, we observe test accuracy for each class without the respect to the number of images for class, as we normalize the results to 1. Confusion matrix demonstrates mistakes in prediction to identify which classes can be invalidly differentiated. We observe that 4% of mistaken class prediction relates to the classes with medium magnesium ions concentrations. Samples with the absence of magnesium ions and its maximum concentration are predicted without mistakes.

Figure 3I presents the correlation between the loss function and training epochs for VGG16 neural network. The error represents the mean absolute error between the values predicted by the CNN and the label values in the validation set. With the increase in the number of epochs, retraining begins, the training accuracy and validation accuracy decrease.

Figure 3I also shows that the loss function of the training set converged faster than the validation set for several of the initial training epochs. After fifteen epochs, the convergence rate of the training and validation sets decreases. The values of error and accuracy of training and validation sets are very close. This indicates that the CNN model has appropriate generalization ability and that there is no evident over-fitting phenomenon in the training.

Therefore, we use VGG16 as the most reliable for the encapsulation system in contrast to other CNNs.

2.3 | Capsules' transformation and cascade of DNA transformation

We investigated the stability of the particles relatively to the environment changes to define whether supramolecular capsule of melamine cyanurate could be destroyed by minor perturbations. Since the M-CA supramolecular assembly is pH-sensitive, we added alkaline solution (NaOH, 0.5 M) to destroy previously formed ssDNA-loaded capsules (Figure 4A). Fluorescence microscopy images of the dismantling process (Figure 4A,B) show a decrease of the fluorescence in RHOD channel both in the center and on the edge of the particles (Supplementary Video 5). Fluorescence-intensity line scans (Figure 4B) associated with the images indicate that the progressive loss of fluorescence intensity correlates with an increase in the fluorescence intensity of the background around the particles. Thus, the performed experiment confirms that ssDNA is released into the gel from the capsules as no other reaction component besides ssDNA modified with TAMRA fluorophore is active in RHOD channel in a dissolved form. Moreover, Figure 4A shows that DNA starts to diffuse into the gel earlier than noticeable particle destruction begins. It indicates also the post-formation ssDNA loading in M-CA capsules.

We also confirm that ssDNA does not undergo degradation or passivation by encapsulation. To characterize functional stability of encapsulated DNA, we used fluorogenic reaction between ssDNA (T-sub) and DNAzyme (Dz1 in Figure 4C). Dz1 consists of two DNA fragments complementary to T-sub that flank the catalytic core of 10–23 DNAzyme, responsible for the cleavage of phosphodiester bond between ribonucleotides g and u.[37] T-sub has a fluorophore (TAMRA) and its quencher (BHQ2) attached to DNA's terminus; when the DNA strand is cleaved at g-u site, the fluorophore separates from the quencher and can generate strong fluorescence.[38,39]

T-sub is entrapped in M-CA capsules in the presence of Mg^{2+}, and no luminescence in RHOD channel appears, even in 7 days (Figure 4D, bottom line). After the formation of the particles, we add gel containing Dz[40] to the reaction-diffusion system and monitored it for 7 days. On the fourth day, luminescence in RHOD channel appeared and reached the maximum on the seventh day (Figure 4D, upper line) due to T-sub cleavage and quencher BHQ2 detachment. By using hydrated metal ions to activate nucleophiles and stabilize transition states and provide site-specific attack of a 2′-hydroxyl group on the adjacent 3′-phosphorus resulting in the formation of a 2′,3′-cyclic phosphate and a 5′-hydroxyl group in a phosphate backbone of the nucleotide chain,[41] the reaction confirms ssDNA presence on melamine cyanurate layers, its accessibility for reagents, and further applicability of M-CA in biochemical reactions.

3 | CONCLUSIONS

In summary, we introduce a novel DNA-loading system based on the supramolecular assembly of M-CA. DNA can be released from the capsules by controllable pH change. By controlling diffusion of M and CA we can indicate the effect of the environmental conditions during the assembly for future applications of this approach. The effect is recognized by ML approach. It opens the way to indicate not only the assembly conditions but also the concentration of encapsulated DNA in the nearest future. Moreover, we demonstrate availability of the trapped DNA for further transformations by conducting hybridization and cleavage reactions with it. We propose to use performed capsules for bioanalysis based on DNAzyme cascade reactions. Furthermore, proposed system can be used for multicomponent encapsulation system including different DNA strands. The relatively large size of the

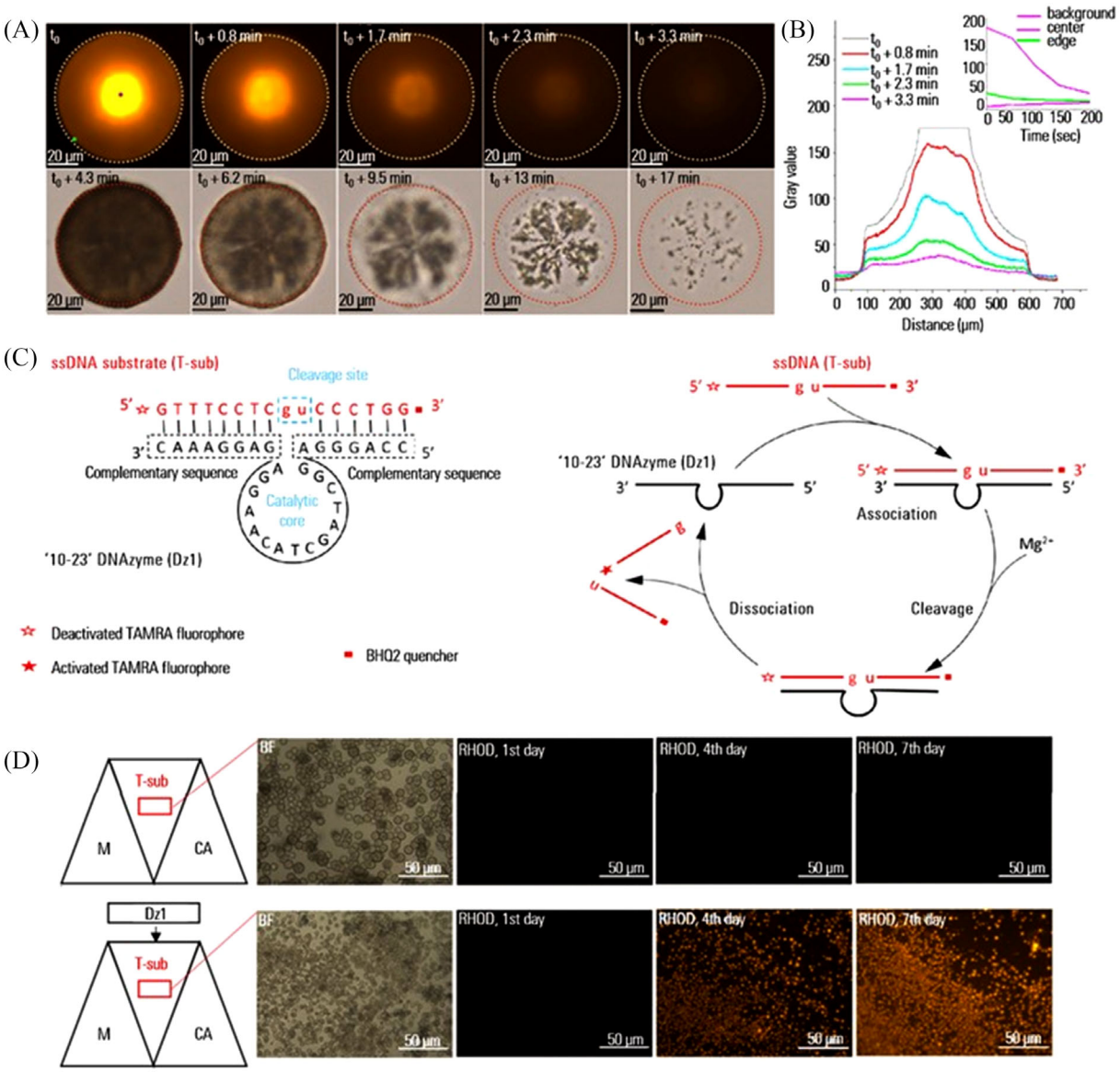

FIGURE 4 Transformation of M-CA capsules and DNA-cascade running. A, Time-dependent microscopy images of the particle disassembly in RHOD channel and bright field (BF). B, Changes in the intensity of fluorescence in the center and at edge of the particle and in the background in RHOD channel. Square dots indicate borders of the particles. Panel presents changes in the fluorescence intensity profile during the particle disassembly in RHOD channel. C, Scheme of biochemical reaction between T-sub and DNAzyme (Dz1) with quencher cleavage. D, Time-dependent reaction-diffusion system with 100 nMT-sub containing gel, and reaction-diffusion system with 100 nM T-sub containing gel and 100 nM Dz1 containing gel, both systems in presence of 50 mM Mg^{2+}: BF, luminescence in RHOD channel after 1, 4, and 7 days. Scale bar 50 μm.

capsules enables its visual identification via simple optical microscopy methods.

4 | METHODS

4.1 | Reagents and materials

Melamine (M, $C_3H_6N_6$) and cyanuric acid (CA, $C_3H_3N_3O_3$) were purchased from Sigma–Aldrich. TAMRA-DNA, T-sub, Dz1e used in this study were synthesized by DNK-sintez, Russia. TAMRA-DNA was purified by polyacrylamide gel electrophoresis (PAGE) and sublimated by DNK-syntez company (Russia, Moscow). An aqueous stock solution of $MgCl_2$(1 M) was prepared from $MgCl_2x6H_2O$ (ACS Grade; purchased from Helicon, Russia). 10× TBE buffer consisted of 89 mM tris, 89 mM boric acid, and 2 mM EDTA in dH_2O (pH = 8.0). Tris, boric acid and EDTA were acquired from Helicon, Russia. dH_2O was prepared using Vent Filter MPK01(TANKMPK01).

NaOH with concentration 0.5 M was prepared from mixing dH_2O and 1 M NaOH. NaOH (1 M) were prepared from *Sodium Hydroxide Fixanal* (LenReactiv, Russia). Agar powder (A7921) was purchased from Sigma–Aldrich.

Acrylamide (AA), bisacrylamide (BA) and urea were purchased from Helicon (Russia). Ammonium persulfate and tetramethyl ethylenediamine were purchased from Carl Roth GmbH (Germany). 40% of AA/BA was prepared from mixing AA and BA in a ratio 29:1 with dH20.

4.2 | Oligonucleotides' preparation

The delivered sublimated TAMRA-DNA (TAMRA - C AGT CGA CTC GCC GAT TAG ACG AAC A) was diluted with Nuclease free-*water* (Invitrogen, USA) to a concentration of 100 μM.

The delivered sublimated T-sub (TAMRA-GTTTCCTC-guCCC TGG-BHQ2) was diluted with Nuclease free-*water* (Invitrogen) to a concentration of 100 μM.

The delivered sublimated Dz1(CCA GGG A GGC TAG CTA CAA CGA GAGGAAAC) was diluted with Nuclease free-*water* (Invitrogen) to a concentration of 100 μM.

4.3 | Fluorescence spectrophotometry assay

The intensity of fluorescence of TAMRA-modified ssDNA was measured by a fluorescence spectrophotometer Aglient Cary 60 (Aglient Technologies, USA). 100 nM TAMRA-DNA was mixed with an analyzing buffer (150 mM KCl, 50 HEPES, 50 MgCl2, 15 mM NaCl, deionized water). The mixture was loaded into a quartz micro cell (Starna GmbH, Germany). A set up for laser wavelengths: excitation = 545 nm; emission = 690 nm.

4.4 | Preparation of agar gels

1 wt% agar gels containing 13 mM M, 100 nM ssDNA and 13 mM CA were prepared in the presence of TBE buffer and required $MgCl_2$ concentration. The final TBE concentration after dilution during gel preparation is 1×. The aqueous solution of $MgCl_2$(1 M) was diluted in 5, 20 and 100 times to get 200, 50 and 10 mM correspondingly after gel preparation. Gels with 500 mM $MgCl_2$ were prepared using $MgCl_2$•6H2O. The mixtures were heated to 100°C to dissolve agar. In contrast to M and CA, ssDNA solution is added after gel cooling to ~ 40°C not before components mixing. The procedure for T-sub and Dz1 containing gels is the same.

4.5 | Formation of particles

Hot gels were poured in glass cuvettes (Figure S1A,B) and left till complete gelation. Melamine, ssDNA and cyanuric acid gels with required size and form were completed and combined in the reaction-diffusion system on glass slide (M, ssDNA, CA gels from left side to right side). (Figure S1C). Particles began to occur almost few minutes later. Samples were left till complete particles formation with provided extra humidity to prevent gel drying.

4.6 | Purification

Gel with formed particles was put into centrifuge tube filled with dH_2O. Then, it was heated using water to dissolve gel. Then, samples were centrifuged, a supernatant was removed and dH_2O was added to a precipitate. Heating and centrifuging were repeated twice to get water solution with pure precipitate.

4.7 | Fluorescence images

Fluorescence microscopy images were obtained using Leica DMI8 microscope equipped with RHOD filter. Images were made in BF and RHOD channels. Acquisition parameters in BF mode: intensity = 100, gain = 1, aperture = 16. Acquisition parameters in RHOD channel: FIM = 100, gain = 1, Il-Fl = 4.

4.8 | Assembly video

To find forming particles RHOD channel was used with FIM = 100%. When bright dots were observed, FIM was decreased to 17%. Images were captured every 15 seconds. Exposure and Il-Fl were 50 ms and 4 correspondingly. For BF the procedure was repeated, but a switch to BF instead of FIM decreasing. Images were captured also every 15 seconds. Acquisition parameters: intensity = 100, gain = 1, aperture = 16. Videos were compiled using Adobe Premier (https://adobe.ly/2FNU63r).

4.9 | Disassembly video

We focused on a chosen area adjusting FIM to 100 and exposure to 100 ms. Then, 0.5 mM NaOH was dropped to cover glass slide around the sample. When particles near chosen area dissolved, image capture started in every 5 seconds. The acquisition parameters were as same as during

the assembly process. For the BF the procedure was the same. Videos were compiled from acquired images using Adobe Premier (https://adobe.ly/2FNU63r).

4.10 | Fluorescence during the assembly

To study changes in fluorescence of a particle ImageJ program package was used. Fluorescence intensity profiles of particles were extracted. Profiles plot was made using OriginLab program package. For the average intensity profiles several particles were analyzed, and resulting profiles were averaged using OriginLab.

4.11 | Fluorescence during the disassembly

The procedure was the same as for assembly. The values of fluorescence intensity in the center and at the edge of the particle and background were measured pointwise.

4.12 | Size and the number of particles

To count particles and measure their size several images of each sample were analyzed using ImageJ program package. Images were from the same gel section. The circularity parameter was set 0.7–1.0.

4.13 | Scanning electron microscopy (SEM) and energy-dispersive X-ray analysis (EDX)

SEM images were obtained using a Hitachi S-3400N (Japan) equipped with Oxford X-Max 20 (UK) EDX spectrometer. Acquisition conditions were as follows: 20 kV accelerating voltage, 1 nA beam current, 60 secconds per spectrum in point mode, 10 kV; 1 nA and 90 minutes acquisition time for mapping. The samples were coated with 2 nm of carbon.

4.14 | PAGE electrophoresis

Denaturing PAGE (Figure S6) was performed using Mini-PROTEAN vertical electrophoresis system (BIORAD) at 80 V (constant voltage) for 2 hours. Gel contained 15% polyacrylamide (40% AA/BA), 7 M Urea, 1× TBE, 10% ammonium persulfate (ACS)(100 µl/10 ml of the gel solution) and TEMED (10 µl/10 ml of the gel solution). 5 µl of 0.5 M NaOH was added to 20 µl water solution with purified particles and left for 5 minutes. After we added 5 µl of 0.5 M HCl to neutralize NaOH and 20 µl of a loading buffer (8 M Urea, 15% 2× TBE). Each lane contained 20 µl of the final solution.

4.15 | Molecular dynamics (MD) simulation details

The classical molecular dynamics (MD) approach is an acceptable method to study the M-CA nucleation processes around ssDNA as well as the influence of cations from atomistic level of description. This method is massively used to study the interactions of simple ions and polycations with DNA.[42–44] It was previously demonstrated[42] that Mg^{2+} make only simultaneous contacts with multiple competing electronegative sites of DNA that last about 1 ns.

ACKNOWLEDGMENTS

The work was carried out with the support of the Ministry of Science and Higher Education of the Russian Federation (agreement № 075-15-2021-1349). The Priority 2030 Federal Academic Leadership Program is acknowledged for infrastructural support. The SEM and EDX studies have been performed in the Centre for Geo-Environmental Research and Modelling of St. Petersburg State University. Support from the Basic Research Program of the National Research University Higher School of Economics is gratefully acknowledged for the part of work on the molecular dynamics models development and the following simulations. The calculations were performed using the resources of HPC facilities at HSE University.[45]

CONFLICT OF INTEREST

The authors declare no conflict of interest.

DATA AVAILABILITY STATEMENT

The data that support the findings of this study are available in the supplementary material of this article.

REFERENCES

1. T. A. Molden, C. T. Niccum, D. M. Kolpashchikov, *Angew. Chem. Int. Ed.* **2020**, *132*, 21376.
2. M. Xiao, W. Lai, T. Man, B. Chang, L. Li, A. R. Chandrasekaran, H. Pei, *Chem. Rev.* **2019**, *119*, 11631.
3. D. Zhang, R. Peng, W. Liu, M. J. Donovan, L. Wang, I. Ismail, J. Li, J. Li, F. Qu, W. Tan, *ACS Nano* **2021**, *15*, 17257.
4. H. Dongran, Q. Xiaodong, M. Cameron, W. Bei, D. Mingjie, J. Shuoxing, B. Maxwell, L. Yan, A. Byoungkwon, Z. Fei, Y. Hao, Y. Peng, *Science* **2017**, *358*, 2648.
5. F. Hong, F. Zhang, Y. Liu, H. Yan, *Chem. Rev.* **2017**, *117*, 12584.
6. A. Joesaar, S. Yang, B. Bögels, A. van der Linden, P. Pieters, B. V. V. S. P. Kumar, N. Dalchau, A. Phillips, S. Mann, T. F. A. de Greef, *Nat. Nanotechnol.* **2019**, *14*, 369.

7. V. Mukwaya, S. Mann, H. Dou, *Commun. Chem.* **2021**, *4*, 161.
8. L. C. Meiser, B. H. Nguyen, Y. J. Chen, J. Nivala, K. Strauss, L. Ceze, R. N. Grass, *Nat. Commun.* **2022**, *13*, 352.
9. Y. Sasaki, D. Miyoshi, N. Sugimoto, *Nucleic Acids Res.* **2007**, *35*, 4086.
10. S. W. Poxon, J. A. Hughes, *Pharm. Dev. Technol.* **2000**, *5*, 115.
11. M. Murakami, *Open Biotechnol. J.* **2013**, *7*, 10.
12. B. Röder, K. Frühwirth, C. Vogl, M. Wagner, P. Rossmanith, *J. Clin. Microbiol.* **2010**, *48*, 4260.
13. N. Deng, W. T. S. Huck, *Angew. Chem. Int. Ed.* **2017**, *129*, 9868.
14. A. A. Nikitina, V. A. Milichko, A. S. Novikov, A. O. Larin, P. Nandi, U. Mirsaidov, D. V. Andreeva, M. V. Rybin, Y. S. Kivshar, E. V. Skorb, *Angew. Chem. Int. Ed.* **2021**, *60*, 12737.
15. W. D. Chen, A. X. Kohll, B. H. Nguyen, J. Koch, R. Heckel, W. J. Stark, L. Ceze, K. Strauss, R. N. Grass, *Adv. Funct. Mater.* **2019**, *29*, 1901672.
16. F. Xia, X. Zuo, R. Yang, Y. Xiao, D. Kang, A. Vallée-Bélisle, X. Gong, J. D. Yuen, B. B. Y. Hsu, A. J. Heeger, K. W. Plaxco, *Proc. Natl. Acad. Sci. U. S. A.* **2010**, *107*, 10837.
17. F. Yamauchi, K. Kato, H. Iwata, *Langmuir* **2005**, *21*, 8360.
18. D. Paunescu, C. A. Mora, M. Puddu, F. Krumeich, R. N. Grass, *J. Mater. Chem. B.* **2014**, *2*, 8504.
19. S. Panicker, I. M. Ahmady, A. M. Almehdi, B. Workie, E. Sahle-Demessie, C. Han, M. M. Chehimi, A. A. Mohamed, *Appl. Organomet. Chem.* **2019**, *33*, 4803.
20. Y. Kamimura, N. Kato, *MATEC Web Conf.* **2017**, *98*, 16.
21. W. Zou, C. Liu, Z. Chen, N. Zhang, *Nanoscale Res. Lett.* **2009**, *4*, 982.
22. X. He, K. Wang, W. Tan, B. Liu, X. Lin, C. He, D. Li, S. Huang, J. Li, *J. Am. Chem. Soc.* **2003**, *125*, 7168.
23. Z. K. Wang, J. Le Lin, Y. C. Zhang, C. W. Yang, Y. K. Zhao, Z. W. Leng, H. Wang, D. W. Zhang, J. Zhu, Z. T. Li, *Mater. Chem. Front.* **2021**, *5*, 869.
24. S. Peng, B. Bie, Y. Sun, M. Liu, H. Cong, W. Zhou, Y. Xia, H. Tang, H. Deng, X. Zhou, *Nat. Commun.* **2018**, *9*, 1293.
25. E. V. Skorb, H. Möhwald, *Adv. Mater.* **2013**, *25*, 5029.
26. V. V. Shilovskikh, A. A. Timralieva, E. V. Belogub, E. A. Konstantinova, A. I. Kokorin, E. V. Skorb, *Appl. Magn. Reson.* **2020**, *51*, 939.
27. B. J. Cafferty, D. M. Fialho, J. Khanam, R. Krishnamurthy, N. V. Hud, *Nat. Commun.* **2016**, *7*, 1.
28. Q. Li, J. Zhao, L. Liu, S. Jonchhe, F. J. Rizzuto, S. Mandal, H. He, S. Wei, H. F. Sleiman, H. Mao, C. Mao, *Nat. Mater.* **2020**, *19*, 1012.
29. N. Avakyan, A. A. Greschner, F. Aldaye, C. J. Serpell, V. Toader, A. Petitjean, H. F. Sleiman, *Nat. Chem.* **2016**, *8*, 368.
30. N. Imoro, V. V. Shilovskikh, P. V. Nesterov, A. A. Timralieva, D. Gets, A. Nebalueva, F. V. Lavrentev, A. S. Novikov, N. D. Kondratyuk, N. D. Orekhov, E. V. Skorb, *ACS Omega* **2021**, *6*, 17267.
31. P. V Nesterov, V. V Shilovskikh, A. D. Sokolov, V. V Gurzhiy, A. S. Novikov, A. A. Timralieva, E. V Belogub, N. D. Kondratyuk, N. D. Orekhov, E. V Skorb, *Symmetry* **2021**, *13*, 1119.
32. M. Lovrak, W. E. J. Hendriksen, C. Maity, S. Mytnyk, V. Van Steijn, R. Eelkema, J. H. Van Esch, *Nat. Commun.* **2017**, *8*, 15317.
33. S. K. Kolev, P. S. Petkov, M. A. Rangelov, D. V. Trifonov, T. I. Milenov, G. N. Vayssilov, *Metallomics* **2018**, *10*, 659.
34. A. N. Petelski, N. M. Peruchena, G. L. Sosa, *J. Mol. Model.* **2016**, *22*, 202.
35. M. Hirohara, Y. Saito, Y. Koda, K. Sato, Y. Sakakibara, *BMC Bioinformatics* **2018**, *19*, 526.
36. A. A. K. Farizhandi, O. Betancourt, M. Mamivand, *Sci. Rep.* **2022**, *12*, 4552.
37. S. Schubert, D. C. Gül, H. P. Grunert, H. Zeichhardt, V. A. Erdmann, J. Kurreck, *Nucleic Acids Res.* **2003**, *31*, 5982.
38. X. Zheng, J. Yang, C. Zhou, C. Zhang, Q. Zhang, X. Wei, *Nucleic Acids Res.* **2019**, *47*, 1097.
39. M. K. Johansson, H. Fidder, D. Dick, R. M. Cook, *J. Am. Chem. Soc.* **2002**, *124*, 6950.
40. H. Rosenbach, J. Victor, M. Etzkorn, G. Steger, D. Riesner, I. Span, *Molecules* **2020**, *25*, 11.
41. D. M. J. Lilley, *Philos. Trans. R. Soc. B Biol. Sci.* **2011**, *366*, 2910.
42. J. Yoo, A. Aksimentiev, *J. Phys. Chem. B* **2012**, *116*, 12946.
43. S. Perepelytsya, *J. Mol. Model.* **2018**, *24*, 171.
44. D. A. Kondinskaia, A. Y. Kostritskii, A. M. Nesterenko, A. Y. Antipina, A. A. Gurtovenko, *J. Phys. Chem. B* **2016**, *120*, 6546.
45. P. S. Kostenetskiy, R. A. Chulkevich, V. I. Kozyrev, *J. Phys. Conf. Ser.* **2021**, *1740*, 12050.

SUPPORTING INFORMATION

Additional supporting information can be found online in the Supporting Information section at the end of this article.

How to cite this article: T. A. Aliev, A. A. Timralieva, T. A. Kurakina, K. E. Katsuba, Y. A. Egorycheva, M. V. Dubovichenko, M. A. Kutyrev, V. V. Shilovskikh, N. Orekhov, N. Kondratyuk, S. N. Semenov, D. M. Kolpashchikov, E. V. Skorb, *Nano Select*. **2022**, *3*, 1526.
https://doi.org/10.1002/nano.202200092